

Hysteresis design of non-stoichiometric Fe₂P-type alloys with giant magnetocaloric effect

Sagar Ghorai,^{1,*} Rebecca Clulow,² Johan Cedervall,² Shuo Huang,^{3,4} Tore Ericsson,²
Lennart Häggström,² Ridha Skini,⁵ Vitalii Shtender,² Levente Vitos,⁶ Olle Eriksson,^{4,7}
Franziska Scheibel,¹ Oliver Gutfleisch,¹ Martin Sahlberg,² and Peter Svedlindh⁵

¹*Institute of Material Science, Technical University of Darmstadt, 64287 Darmstadt, Germany*

²*Department of Chemistry – Ångström Laboratory, Uppsala University, Box 538, SE-751 21 Uppsala, Sweden*

³*Faculty of Materials Science and Chemistry, China University of Geosciences, Wuhan 430074, China*

⁴*Department of Physics and Astronomy, Uppsala University, Box 516, SE-751 20 Uppsala, Sweden*

⁵*Department of Materials Science and Engineering, Uppsala University, Box 35, SE-751 03 Uppsala, Sweden*

⁶*Department of Materials Science and Engineering, Royal Institute of Technology, Stockholm SE-100 44, Sweden*

⁷*Wallenberg Initiative Materials Science for Sustainability, Uppsala University, 75121 Uppsala, Sweden*

(Dated: October 3, 2024)

The non-stoichiometric Fe₂P-type (FeMnP_{0.5}Si_{0.5})_{1-x}(FeV)_x alloys ($x = 0, 0.01, 0.02,$ and 0.03) have been investigated as potential candidates for magnetic refrigeration near room temperature. The magnetic ordering temperature decreases with increasing FeV concentration, x , which can be ascribed to decreased ferromagnetic coupling strength between the magnetic atoms. The strong magnetoelastic coupling in these alloys results in large values of the isothermal entropy change (ΔS_M); 15.7 J/kgK, at 2 T magnetic field for the $x = 0$ alloy. ΔS_M decreases with increasing x . Results from Mössbauer spectroscopy reveal that the average hyperfine field (in the ferromagnetic state) and average center shift (in the paramagnetic state) have the same decreasing trend as ΔS_M . The thermal hysteresis (ΔT_{hyst}) of the magnetic phase transition decreases with increasing x , while the mechanical stability of the alloys improves due to the reduced lattice volume change across the magnetoelastic phase transition. The adiabatic temperature change ΔT_{ad} , which highly depend on ΔT_{hyst} , is 1.7 K at 1.9 T applied field for the $x = 0.02$ alloy.

I. INTRODUCTION

The worldwide use of refrigeration systems consumes about 20% of the world's electricity and is responsible for around 7.8% of the global greenhouse emission [1, 2]. Solid-state refrigeration, based on the magnetocaloric (MC) effect is a more efficient (20 – 30%) and environmentally-friendly alternative cooling technology [3]. Although the first near room temperature giant MC material Gd₅(Si,Ge)₄ was discovered already in 1997, finding a rare-earth free, non-toxic, and economically viable MC material is still a relevant subject for research. Usually, materials with first-order magnetic phase transitions (FMPTs) show a giant MC effect owing to their coupled structural (or lattice) and magnetic degrees of freedom. The FMPT, induced by the coupled magnetic and structural phase changes is generally accompanied by a thermal hysteresis (ΔT_{hyst} , difference in phase transition temperature while cooling and heating the material) related to the latent heat involved in the FMPT. ΔT_{hyst} significantly affects important properties of the MC material; i.e. adiabatic temperature change (ΔT_{ad}), and isothermal entropy change ($-\Delta S_M$) [4]. The most studied MC materials currently include Fe₂P-type [5], LaFe_{13-x}Si_x [6], NiMn Heusler-type [7] and MM'X (M = Fe or Mn, M'=Co or Ni, X=Si or Ge) [8] based alloys. Apart from ΔT_{hyst} , another major drawback of

most FMPT alloys is the mechanical instability related to the lattice volume change (ΔV) during the phase transition. In this regard, Fe₂P-type (Mn,Fe)₂(P,Si) alloys with $\Delta V < 1\%$ and with a largely tunable ΔT_{hyst} [9] are promising candidates for magnetic refrigeration systems. Although the ΔV is negligible in the Fe₂P-type alloys, the lattice parameter ($\Delta(c/a)$) change, plays a crucial role in determining mechanical stability [10].

In our previous work, we observed that 5 at% of stoichiometric V addition in the metallic site of FeMnP_{0.5}Si_{0.5} reduced the magnetic ordering temperature (T_t) by 14% and ΔT_{hyst} by 61% [11]. It has also been observed that non-stoichiometric addition in the metallic site of the (Fe,Mn)₂(P,Si) system can influence the MC effect significantly [12]. However, the effect of non-stoichiometry in the P/Si site, often caused by P-loss during the synthesis process is still unexplored [13]. Moreover, Dung *et al.* [14] have shown that the MC effect in the (Fe,Mn)₂(P,Si)-system depends on the drastic change of the Fe-moment at the magnetic phase transition, changing from weak itinerant magnetism in the paramagnetic (PM) state to a sizeable localized magnetic moment in the ferromagnetic (FM) state. The degree of localization of Fe-moments in the PM state is expected to increase if the overlap between the 3d and 2p orbitals of Fe and P/Si decreases, which in turn should have an impact on the change of the Fe-moment at the magnetic phase transition and hence also on the MC effect. A site-specific Fe-moment fluctuation has also been found in calculations for the pure Fe₂P-compound [15]. Therefore, non-stoichiometric addition in the P/Si-site may also in-

* e-mail: sagar.ghorai@tu-darmstadt.de

fluence the MC effect by changing the metal to non-metal ratio in the alloy.

This study focuses on the effect of Fe-moment localization on the MC effect, as well as on reducing ΔT_{hyst} , in non-stoichiometric $(\text{FeMnP}_{0.5}\text{Si}_{0.5})_{1-x}(\text{FeV})_x$ alloys ($x = 0, 0.01, 0.02, \text{ and } 0.03$). In addition, the effect of non-stoichiometry on ΔV , and $\Delta(c/a)$ associated with the magnetoelastic transition and its influence on the mechanical stability of the alloys is investigated.

II. EXPERIMENTAL DETAILS AND CALCULATION METHOD

Master alloys of $\text{FeMnP}_{0.5}\text{Si}_{0.5}$ and FeV were synthesized by drop synthesis [13] and conventional arc-melting, respectively. Further, stoichiometric amounts of the two master alloys were mixed by hand grinding, pressed into pellets, and vacuum sealed in quartz tubes. The vacuum-sealed alloys were sintered at 1373 K for 1 hr and at 1073 K for 65 hr, followed by quenching in ice water. Four samples were synthesized in this way; $(\text{FeMnP}_{0.5}\text{Si}_{0.5})_{1-x}(\text{FeV})_x$, with $x = 0, 0.01, 0.02$ and 0.03 .

Temperature dependent X-ray powder diffraction (XRPD) data were collected using a Bruker D8 Advance diffractometer with $\text{Cu-K}\alpha_1$ radiation, and the data were analyzed using Pawley refinements within the Topas6 software [16]. The energy dispersive X-ray spectroscopy (EDX) measurements were performed on a Zeiss Leo 1550 instrument with an Aztec energy dispersive X-ray detector. A constant acceleration spectrometer with $^{57}\text{CoRh}$ source was used for the collection of Mössbauer spectra at 410 K and 100 K. The spectra were folded and fitted using the least square Mössbauer fitting program "Recoil". The magnetic properties were investigated in the temperature range from 5 K to 400 K using Quantum Design MPMS-XL and PPMS systems with a maximum magnetic field of 5 T. The adiabatic temperature change (ΔT_{ad}) was measured in the temperature range from 220 K to 380 K, with a maximum applied field of 1.9 T in a home-built device at the Technical University of Darmstadt, Germany [17].

Density functional theory [18] calculations were carried out by the exact muffin-tin orbitals method [19]. The one-electron Kohn-Sham equations were solved within the soft-core and scalar-relativistic approximations. The self-consistent calculations were performed with the local-density approximation by Perdew and Wang [20], and the total energy calculations were performed with the generalized-gradient approximation by Perdew, Burke, and Ernzerhof [21]. The Green's function was calculated by using 16 complex energy points on a semicircular contour including the valence states. The chemical disorder was treated by the coherent-potential approximation [22]. The PM state was simulated by the disordered local moments approximation [23]. Further details about the adopted methods can be found in previous work [19].

III. PHASE STABILITY

Total energy calculations for the studied alloys were performed to check the phase stability and the site preference of the atoms. From previous studies [11, 24] it

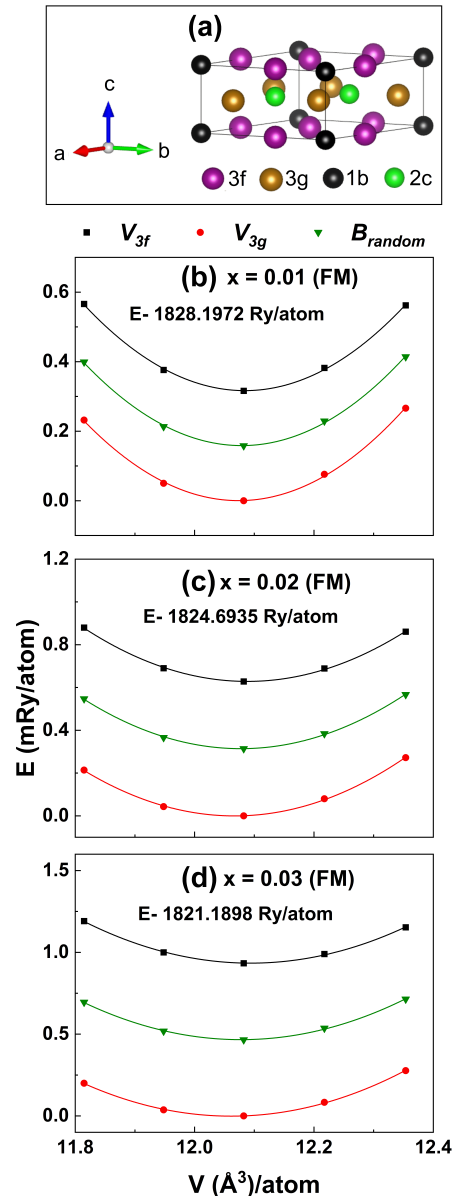


FIG. 1. (a) Hexagonal structure of the $\text{FeMnP}_{0.5}\text{Si}_{0.5}$ alloy obtained from XRPD refinement; the different crystallographic sites are color coded. (b)-(d) The calculated total energy as a function of the lattice volume in the FM state of the studied alloys. The energy values are rescaled (see inset formula) with respect to the minimum total energy of the corresponding alloy. The color coded lines joining the data points are polynomial fits to the corresponding data.

is known that Fe, Mn, and P/Si prefer to occupy the $3f$, $3g$, and $1b/2c$ crystallographic sites in the hexagonal Fe_2P -type structure, respectively (cf. Fig. 1 (a)).

For the total energy calculation, four possible cases have been considered: (i) V occupies only the $3f$ site (V_{3f}); (ii) V occupies only the $3g$ site (V_{3g}); (iii) Fe, Mn and V randomly occupy the $3f$ and $3g$ sites (A_{ran}); and (iv) Fe and Mn from the Fe_2P -type phase occupy the $3f$ and $3g$ sites, respectively, while Fe and V from the FeV phase occupy the $3f$ and $3g$ sites randomly (B_{ran}). The total energy values as a function of lattice volume for all cases in the FM state are shown in Fig. 1 (b)-(d). Owing to the relatively higher total energy values, the A_{ran} -case has been excluded from Fig. 1 (b)-(d). In addition, for better comparison between different cases, the total energy values are shifted by the minimum energy (see insets of Fig. 1 (b)-(d)) of each corresponding alloy. The minimum energy is observed for the V_{3g} case, i.e. when V occupies only the $3g$ site. Noticeably, the relative energy difference increases with increasing x , confirming a more stable V occupancy in the $3g$ site. A similar $3g$ site preference of V is also calculated for the PM state (see SI). In addition to the total energy calculation, the formation energy calculation of the $FeMnP_{0.5}Si_{0.5}{}_{1-x}(FeV)_x$ alloy, indicates a $3g$ -site preference of V, which is discussed in the SI.

IV. RESULTS AND DISCUSSION

A. Chemical composition analysis

The chemical compositions and homogeneity of the alloys have been verified by EDX analysis. Owing to the porous and brittle nature of the alloys, the possibility to resolve proper phase boundaries is limited. However, from the elemental mapping of the studied alloys, apart from the main Fe_2P -type phase, a small amount of secondary phase with P- and Mn-deficiency has been observed (see highlighted regions in Fig. 2 (a)-(d)). The elemental at% of the main Fe_2P -type phase is shown in Fig. 2 (e). The variation of V in the alloys is as expected, while the amount of Fe in the main phase is lower than expected, indicating that Fe is involved in the formation of the secondary phase. The observed chemical composition of the secondary phase is; Fe 44(4) at%, Mn 30(3) at%, P 8.3(8) at% and Si 18(2) at% for the $x = 0$ alloy. A similar P-deficient secondary phase is also observed for the rest of the alloys. From XRPD analysis (will be discussed later), this secondary phase is identified as a $(Fe,Mn)_3Si$ -type phase which is also observed for stoichiometric V added alloys [11].

B. Coupled structural and magnetic phase transition

The analysis of the temperature dependent XRPD data (see SI Fig. 2) reveals a hexagonal Fe_2P -type structure with space group $P\bar{6}2m$ for the studied alloys. Although the hexagonal structure remains unchanged, the

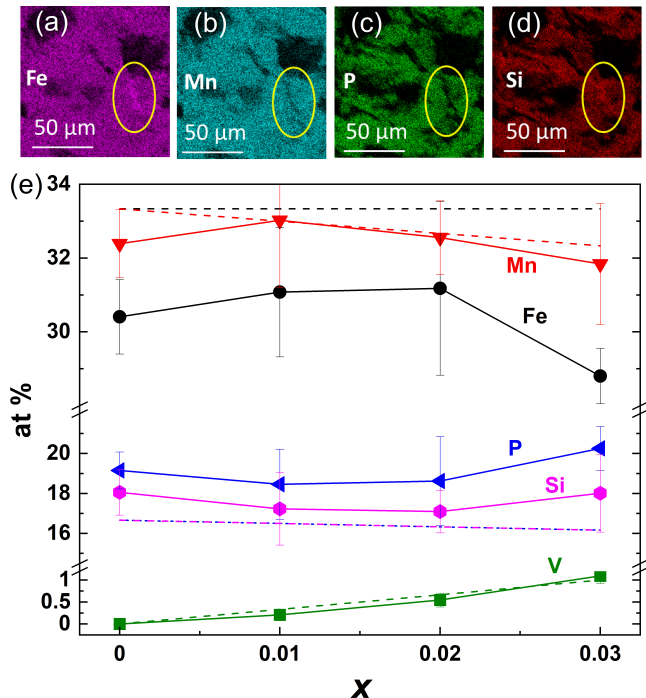


FIG. 2. (a)-(d) Elemental mapping of the $x = 0$ alloy. The area marked with a yellow ellipse represents the secondary phase. A brighter (darker) color indicates an increased (decreased) amount of the element. (e) Variation of elemental at% with x . The dotted lines with same color indicate the desired at% of the element in the $(FeMnP_{0.5}Si_{0.5})_{1-x}(FeV)_x$ alloys. The error bars correspond to standard deviations of 10 successive measurements.

c/a -ratio exhibits a strong change with temperature in the magnetic transition region (to be discussed later), which is often referred to as a magnetoelastic phase transition. With decreasing temperature, the c/a -ratio changes from a high (≈ 0.57) to a low (≈ 0.53) value (see Fig. 3(a) and (b)). During this lattice parameter change, there is also a change of lattice volume (ΔV), as shown in the inset of Fig. 3 (a). ΔV is defined as the volume difference between the low and high c/a -ratio phases. The value of ΔV decreases with increasing x , except for the $x = 0.03$ alloy. The lattice parameter change is accompanied by a magnetic phase transition (PM to FM phase, cf. Fig. 3(c)), enabling coupled magnetic and lattice entropy changes. The sharpness of the c/a -ratio change across the transition region indicates the strength of the magnetoelastic phase transition, which can be defined as [11],

$$\Delta(c/a)(\%) = \lim_{T \rightarrow T_t} \frac{(c/a)_{PM} - (c/a)_{FM}}{(c/a)_{PM}} \times 100, \quad (1)$$

where $(c/a)_{PM}$ and $(c/a)_{FM}$ correspond to the (c/a) -ratio just above and below the magnetic ordering temperature T_t , respectively. From the inset of Fig. 3 (b),

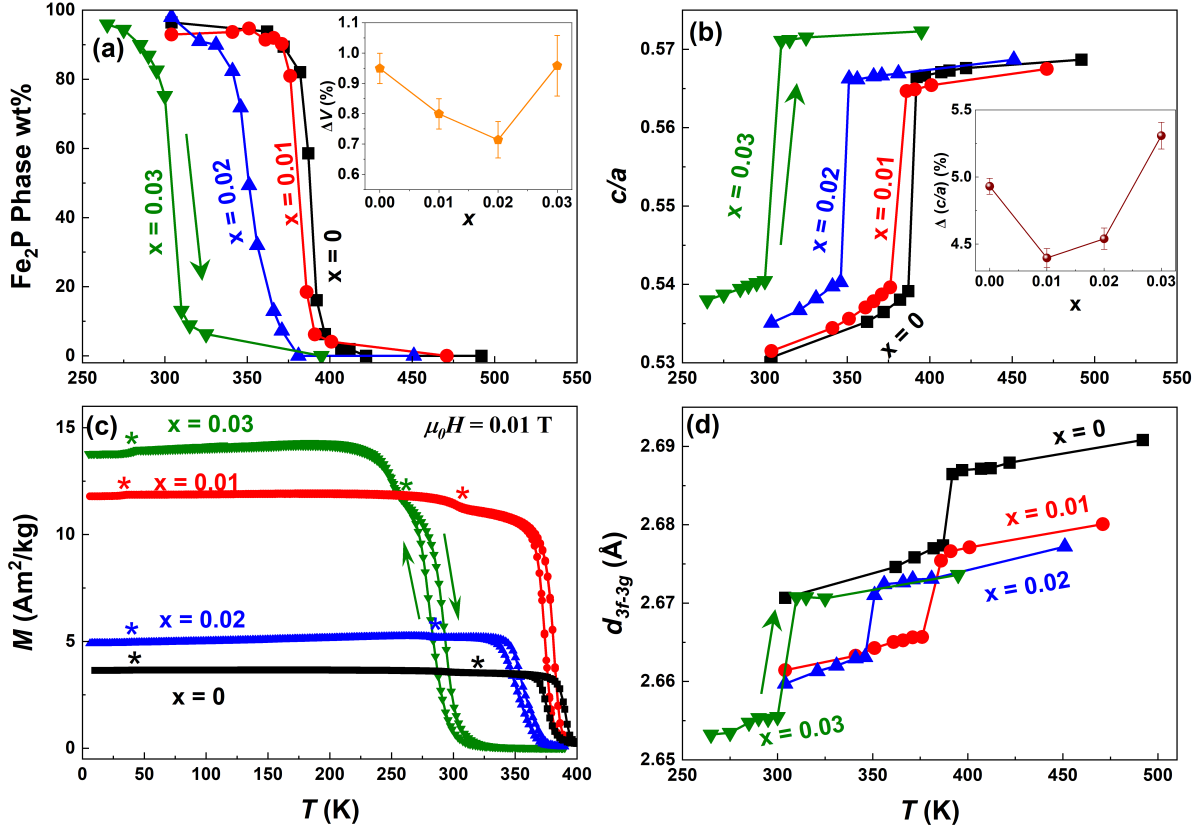


FIG. 3. (a) Temperature dependence of the low c/a -ratio (≈ 0.53) Fe_2P -phase, data recorded during heating; the inset shows the change in lattice volume ΔV in the transition region versus x , being defined as the difference in lattice volume between the low and high c/a -ratio phases. (b) c/a -ratio versus temperature considering only the dominating Fe_2P -phase (wt% $> 60\%$) during heating. The calculated error from the XRPD refinement of the lattice parameter data is in the order of 10^{-4} Å. The inset shows the change of the c/a -ratio versus x in the magnetic transition region. (c) Magnetization versus temperature at $\mu_0 H = 0.01$ T; the kinks in the magnetization curves (marked with *) originate from the magnetic secondary phase. (d) Atomic distance between the $3f$ and $3g$ sites versus temperature.

the largest (smallest) change of the (c/a) -ratio has been observed for the $x = 0.03$ ($x = 0.01$) alloy.

The value of T_t decreases as expected with increasing V addition in the metal site of the alloy (cf. Fig. 3(c)). However, one should keep in mind that the non-stoichiometry in the non-metal site also influences T_t . As a comparison, with 5 at% stoichiometric V addition, T_t decreased by 14%, while in the present study, with 3 at% non-stoichiometric V addition T_t decreases by 25% [11]. This additional decrease of T_t is the result of the non-stoichiometry in the non-metal site. The XRPD analysis reveals that apart from the principle Fe_2P -type hexagonal phase all samples contain the $(\text{Fe,Mn})_3\text{Si}$ -type secondary phase. However, the parent alloy additionally contains a small amount (3 wt%) of a Mn_5Si_3 -type secondary phase, which is negligible in the FeV added alloys (see SI Fig. 3). With increasing x , there is an almost linear increase of the $(\text{Fe,Mn})_3\text{Si}$ phase (from 3.1 wt% in the $x = 0$ alloy to 9.2 wt% in the $x = 0.03$ alloy). This secondary phase is magnetic, the small kinks observed in the temperature dependent magnetization curves (cf.

Fig. 3(c)) below T_t originate from this secondary phase [11, 25]. The anomalous ΔV and $\Delta(c/a)$ values for the $x = 0.03$ alloy (cf. insets of Fig. 3 (a) and (b)) is mostly the result of the larger weight-% of the secondary phase. The same secondary phase has also been observed for stoichiometrically V added $\text{FeMnP}_{0.5}\text{Si}_{0.5}$ alloys. However, with stoichiometric V addition, the amount of the secondary phase was almost constant [11]. Irrespective of the metal to non-metal ratio, the presence of the secondary phase will decrease the Si/P ratio in the alloy. Previously, a decrease of T_t has been observed with decreasing Si/P ratio [14, 26], without providing an explanation for the Si/P ratio dependence of T_t .

The magnetic transition temperature of Fe_2P -type alloys is often related to the atomic distance between the magnetic atoms situated in the $3f$ and $3g$ sites [11]. From the XRPD data refinement, the positions of the $3f$ and $3g$ sites atoms (cf. Fig. 1) are $(x, 0, 0)$, and $(y, 0, 0.5)$, respectively. Using these values, the interatomic distance (d_{3f-3g}) between the $3f$ and $3g$ sites atoms is calculated

as [27],

$$d_{3f-3g} = \sqrt{[(y-x) \times a]^2 + [0.5 \times c]^2}. \quad (2)$$

The values of d_{3f-3g} are shown in the Fig. 3 (d). It is clear that the values of d_{3f-3g} decrease with increasing x following a similar trend as T_t .

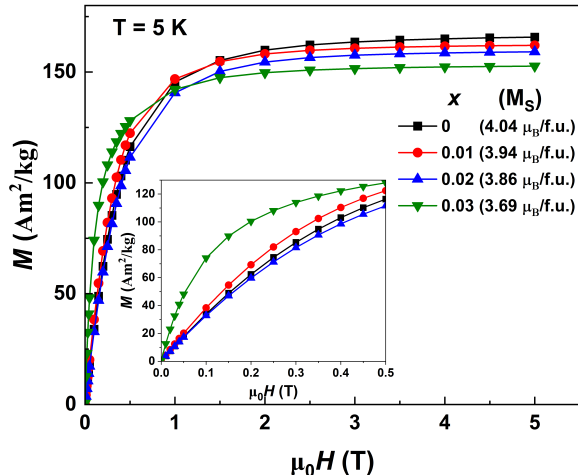


FIG. 4. Magnetic field dependent magnetization at 5 K temperature. The inset highlights the low-field region.

The saturation magnetizations (M_S) for the studied alloys are estimated from the magnetic field dependent magnetization measurement at 5 K temperature (cf. Fig. 4). With increasing x , the decrease of M_S , results from the replacement of magnetic atoms (Mn, or Fe) with non-magnetic V atoms. Interestingly, the magnetization at lower fields does not follow the trend of the M_S , and indicates a change in magnetic anisotropy with x .

C. Magnetocaloric effect and thermal hysteresis

The MC effect can be quantified by the isothermal magnetic entropy change (ΔS_M) of the system. For a magnetic field change from zero to H_f , ΔS_M can be expressed using Maxwell's relation as [28],

$$\Delta S_M(T, H_f) = -\mu_0 \int_0^{H_f} \left(\frac{\partial M}{\partial T} \right)_H dH. \quad (3)$$

The calculated values of ΔS_M for the studied alloys are shown in Fig. 5(a). A decrease of ΔS_M with increasing x is observed. In our previous work [11], for the stoichiometrically V added $\text{FeMnP}_{0.5}\text{Si}_{0.5}$ alloys, it was observed that the value of ΔS_M is directly proportional to the strength of the magnetoelastic coupling. The strength of the magnetoelastic coupling is defined by the relative change of the hexagonal lattice parameters. In this work, the relative change of the c/a -ratio at the magnetic transition is highest for the $x = 0.03$ alloy (cf. inset of Fig. 3(b)). However, the trend of ΔS_M does not follow the

lattice parameter change. Therefore, the magnetoelastic coupling strength can not be described from the lattice parameters of the non-stoichiometric Fe_2P -type alloys, especially when there is a magnetic secondary phase involved.

Since the total entropy during an adiabatic process is conserved, the change of magnetic entropy by the application or removal of a magnetic field will change the phonon entropy of the system. This change of phonon entropy will also change the temperature of the system, known as the adiabatic temperature change (ΔT_{ad}), the most important parameter for characterization of the MC effect [29]. For a system with a heat capacity of $C(H, T)$, ΔT_{ad} for a magnetic field change from zero to H_f can be expressed as [30],

$$\Delta T_{ad}(T, H_f) = -\mu_0 \int_0^{H_f} \left(\frac{T}{C} \right)_H \left(\frac{\partial M}{\partial T} \right)_H dH. \quad (4)$$

From Eq. 3, it is clear that at a particular temperature, $-\Delta S_M$ depends both on the magnitude of the magnetization and rate of change of the magnetization with respect to temperature. In addition to this, Eq. 4 indicates that a smaller heat capacity yields a larger ΔT_{ad} . In this work, the ΔT_{ad} has only been measured for the $x = 0.02$ alloy, as the rest of the alloys were extremely brittle, implying that ΔT_{ad} of these samples could not be measured with our setup where physical contact between the sample and the thermocouple is required. This mechanical instability of the three alloys can also be related to the relatively large value of ΔV (cf. inset of Fig. 3 (a)). The MC effect properties of the studied alloys are compared in Table I with well-known giant MC materials with magnetic phase transitions near room temperature.

TABLE I. Magnetocaloric properties of the studied alloys (*) compared with data reported for other giant MC materials near room temperature. The ΔS_M values correspond to a $\mu_0 H = 2\text{T}$ field change. The values of T_t for the studied alloys are taken from the field cooled (FC) magnetization versus temperature curves at $\mu_0 H = 0.01\text{T}$.

Sample	T_t (K)	$-\Delta S_M$ (J/kg)	ΔT_{ad} ($\mu_0 H$) (K)	Ref.
$\text{FeMnP}_{0.5}\text{Si}_{0.5}$	376	16.5	-	*
$(\text{FeMnP}_{0.5}\text{Si}_{0.5})_{0.99}(\text{FeV})_{0.01}$	374	14.8	-	*
$(\text{FeMnP}_{0.5}\text{Si}_{0.5})_{0.98}(\text{FeV})_{0.02}$	348	7.8	1.7 (1.9 T)	*
$(\text{FeMnP}_{0.5}\text{Si}_{0.5})_{0.97}(\text{FeV})_{0.03}$	281	7.7	-	*
$\text{FeMn}_{0.95}\text{V}_{0.05}\text{P}_{0.5}\text{Si}_{0.5}$	322	13.1	-	[11]
$\text{Fe}_{0.95}\text{V}_{0.05}\text{Mn}_{0.5}\text{P}_{0.5}\text{Si}_{0.5}$	318	9.1	-	[11]
$\text{Fe}_{0.71}\text{Mn}_{1.32}\text{P}_{0.5}\text{Si}_{0.56}$	265	16	2.35 (1.9 T)	[31]
$\text{Fe}_{0.975}\text{Mn}_{0.975}\text{P}_{0.47}\text{Si}_{0.5}\text{B}_{0.03}$	329	11.6	1.9 (2 T)	[32]
$\text{Fe}_{0.84}\text{Co}_{0.11}\text{Mn}_{0.51}\text{Si}_{0.45}\text{B}_{0.04}$	295	11.4	1.9 (1.1 T)	[33]
$\text{FeMnP}_{0.45}\text{As}_{0.55}$	306	10.7	2.9 (1.1 T)	[34]
$\text{Ni}_{45.2}\text{Mn}_{36.7}\text{In}_{13}\text{Co}_{5.1}$	311	~ 19	6.2 (1.9 T) 1.5 (-1.9 T)	[17]
$\text{La}_{0.4}\text{Pr}_{0.3}\text{Ca}_{0.1}\text{Sr}_{0.2}\text{MnO}_3$	289	3.08	1.5 (1.9 T)	[35]
Gd	295	6.1	5.5 (1.9 T)	[36]

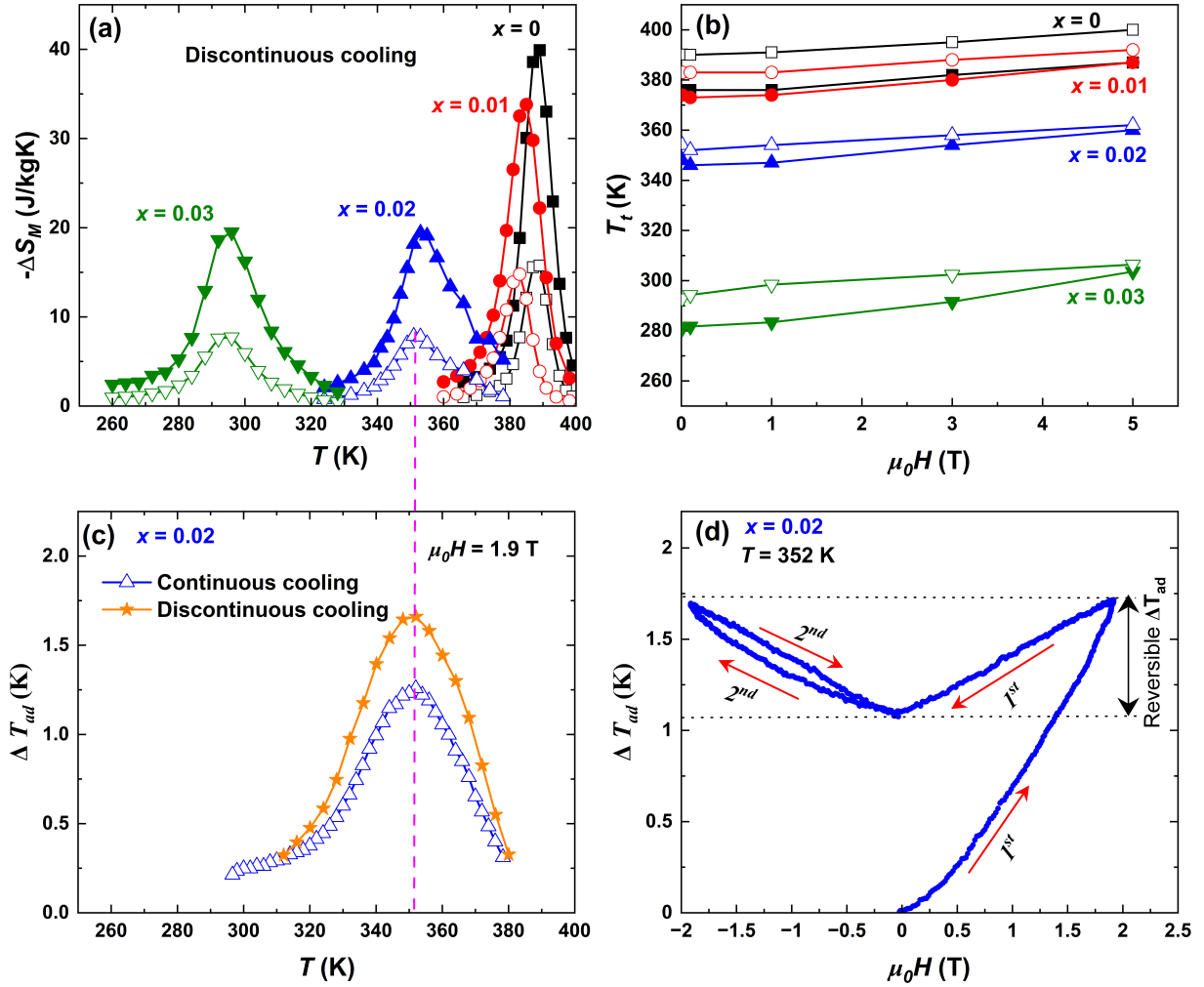


FIG. 5. (a) Temperature dependent isothermal entropy change measured at 2 T (hollow symbols) and 5 T (solid symbols) applied fields, respectively. (b) T_t versus magnetic field, solid (hollow) symbols correspond to data recorded during cooling (heating). (c) Temperature dependent adiabatic temperature change for the $x = 0.02$ alloy, measured at $\mu_0 H = 1.9$ T following continuous cooling (hollow symbols) and discontinuous cooling (solid symbols) protocols. (d) Magnetic field dependent irreversibility of ΔT_{ad} at 352 K. Arrows indicate the direction of magnetic field change.

The observed values of ΔT_{ad} for the $x = 0.02$ alloy, measured following continuous cooling and discontinuous cooling (where the sample is heated to its PM state before approaching the measuring temperature) protocols are shown in Fig. 5 (c). The large difference between measured ΔT_{ad} values, following the continuous cooling and discontinuous cooling protocols, is due to the thermal hysteresis ΔT_{hyst} of the alloy [4]. To understand the effect of ΔT_{hyst} , the field dependence of ΔT_{ad} is shown at a temperature (352 K) near the T_t of the alloy. Before this measurement, the sample was heated to its PM state, i.e. ΔT_{ad} was recorded following the discontinuous protocol. While cooling from the PM state, in the vicinity of T_t , the sample will undergo a magnetic phase transition coupled with a structural (in this case a c/a -ratio change) phase transition. As shown in Fig. 5 (d), starting from zero magnetic field and increasing the field

to 1.9 T the temperature of the sample increases by 1.7 K, but removal of the field does not bring the sample back to its initial temperature. However, applying and removing the same field (this time -1.9 T) a second time will bring the sample back to the same temperature as obtained after the first field cycle. In this sense ΔT_{ad} is reversible during the second field cycle. The irreversible behaviour of ΔT_{ad} is a result of the coupled magnetic and structural phase changes; as the structural phase change is irreversible, ΔT_{ad} will also be irreversible during the first cycle. Mostly, the residual heat after the first cycle represents the latent heat for the structural phase change. During the second magnetic field cycle, the applied field can not overcome ΔT_{hyst} , as a result, the magnetoelastic phase transition is not complete. Similar results have been observed for the Ni-Mn-In-Co Heusler compound [38].

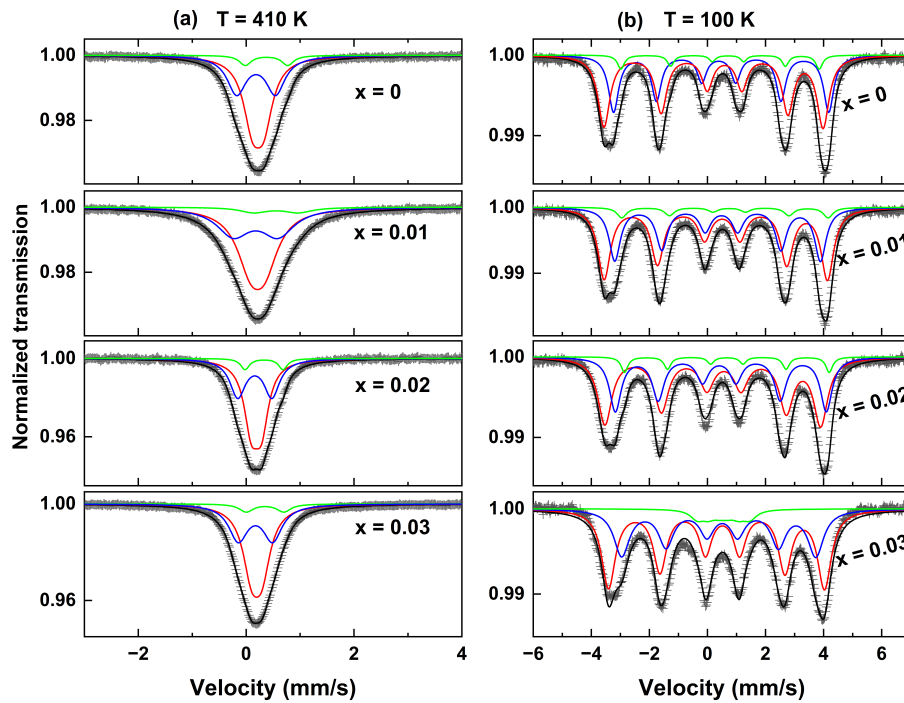


FIG. 6. Mössbauer spectra at (a) 410 K and (b) 100 K. The red, blue, and green sub-patterns correspond to the nearest neighbour surroundings, $\text{Fe}_{2\text{P}2\text{Si}}$, $\text{Fe}_{3\text{P}1\text{Si}}$, and $\text{Fe}_{4\text{P}}$ of Fe at the $3f$ site, respectively.

The field dependence of T_t during heating and cooling is shown in Fig. 5(b). The temperature region between the heating and cooling curves corresponds to a mixed paramagnetic-ferromagnetic state defining ΔT_{hyst} . The lowest value of ΔT_{hyst} is observed for the $x = 0.02$ alloy. To predict the tricritical point where $\Delta T_{hyst} = 0$, a linear extrapolation of the data in Fig. 5(b) yields the critical temperature (T_{crit}) and critical field ($\mu_0 H_{crit}$) for each alloy, except for the $x = 0$ alloy for which the used magnetic field range was not sufficient to make this analysis meaningful. A $\mu_0 H_{crit}$ value of 10 T is obtained for the $x = 0.01$ alloy, while $\mu_0 H_{crit} \approx 6$ T is obtained for the $x = 0.02$ and $x = 0.03$ alloys, with the corresponding T_{crit} values being 404 K, 365 K and 309 K, respectively.

D. Hyperfine interaction

From the previous discussion, it is clear that for non-stoichiometric Fe_2P -type alloys the magnetoelastic coupling strength, derived from the lattice parameter change at T_t , can not properly describe the difference in ΔS_M between the alloys. The large ΔS_M values of the $(\text{Fe},\text{Mn})_2(\text{P},\text{Si})$ alloys are often ascribed to the Fe-moment fluctuation at T_t and its hybridization with the non-metallic atoms in the alloy [14]. Mössbauer spectra in the PM (410 K) and FM (100 K) states of the studied alloys have been collected to investigate the hyperfine interaction of Fe with its neighboring atoms; the results

are presented in Fig. 6 (a) and (b), respectively.

From the spectra recorded at 410 K, the strong $3f$ site preference for Fe is confirmed by the absence of any secondary line at higher velocity [39]. All 410 K spectra irrespective of V content were fitted with three doublets corresponding to three possible nearest neighbor interactions of the Fe atom. These are one Fe atom surrounded by two P and two Si atoms ($\text{Fe}_{2\text{P}2\text{Si}}$), three P and one Si atom ($\text{Fe}_{3\text{P}1\text{Si}}$), and four P atoms ($\text{Fe}_{4\text{P}}$) with probabilities 0.5625, 0.375 and 0.0625, respectively. The probabilities are calculated using the site preference for the $2c$ site for Si [24]. To shed light on the Fe-moment localization and its variation with x , the average center shift (CS) at 410 K and the average hyperfine field (B_{hf}) at 100 K are presented in Fig. 7. The reported CS values have natural α -Fe at 295 K as a reference absorber. The average CS value decreases with increasing x . This decrease corresponds to an enhanced electron density at the Fe nuclei, which indicates a stronger orbital overlap between the $3d$ and $2p$ orbitals of the Fe and P/Si atoms. As mentioned in the introduction, the large value of ΔS_M in the $(\text{Fe},\text{Mn})_2(\text{P},\text{Si})$ alloys can be ascribed to the drastic change of the Fe-moment (from $\approx 0.003\mu_B/\text{atom}$ to $1.54\mu_B/\text{atom}$) at T_t [14], something which is consistent with results from theoretical calculations [15]. From the observed values of CS , the tendency for localization of the Fe-moments decreases with increasing x , which suggests a suppressed change of the Fe-moment at the magnetic transition. With increasing x (cf. Fig. 7), the

gradual decrease of B_{hf} in the FM region indicates a decrease of the local magnetization of Fe, which is also in agreement with the decrease of ΔS_M [39].

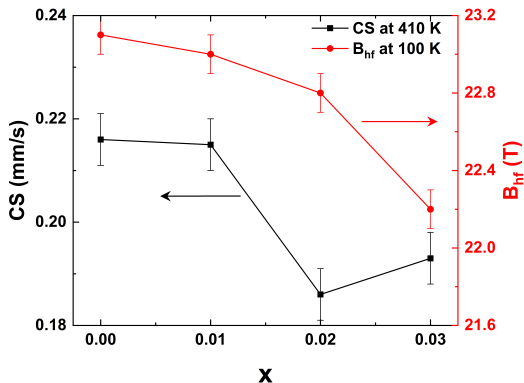


FIG. 7. Average CS and B_{hf} values obtained from Mössbauer spectra at 410 K and 100 K, respectively. For details see main text.

It is important to keep in mind that the amount of secondary phase increases with increasing x . However, the effect of the secondary phase on the Mössbauer spectra is not obvious.

V. CONCLUSIONS

The magnetic and magnetocaloric properties of $(\text{FeMnP}_{0.5}\text{Si}_{0.5})_{1-x}(\text{FeV})_x$ alloys, with $x = 0, 0.01, 0.02$ and 0.03 , have been investigated. From the formation energy calculations, it was found that V has a preferred $3g$ -site occupancy in the Fe_2P type hexagonal structure. The studied alloys exhibit temperature dependent magnetoelastic phase transitions, from the low-temperature hexagonal phase with a low c/a -ratio to the high-temperature hexagonal phase with a high c/a -ratio. Similar to the non-stoichiometry in the metallic site of $(\text{Fe,Mn})_2(\text{P,Si})$ alloys, the non-stoichiometry in the non-metallic site also influences the secondary $(\text{Fe,Mn})_3\text{Si}$ -type phase formation [12]. A decrease of the phase transition temperature with increasing x is observed, which is an effect of decreased FM exchange interaction between the magnetic atoms (Fe and Mn). The $3f$ -site prefer-

ence of the Fe-atom has been confirmed from analysis of the Mössbauer spectra. In addition, the analysis of the Mössbauer spectra has revealed an enhanced electron density at the Fe nuclei with increasing x . Moreover, with increasing x , the B_{hf} and the saturation magnetization decreases gradually, providing an explanation for the decrease of ΔS_M .

For stoichiometric V addition in the $\text{FeMnP}_{0.5}\text{Si}_{0.5}$ alloys, the variation of ΔS_M can be directly related to the variation of the magnetoelastic coupling strength, which is given by the relative change of the hexagonal lattice parameters at T_t [11]. However, in the case of non-stoichiometric V addition, a secondary phase will form in the alloy. Thus, the magnetoelastic coupling strength can not be directly related to the relative change of lattice parameters in the studied alloys. A magnetic field dependent irreversible variation of the ΔT_{ad} has been observed for the $x = 0.02$ alloy. The associated ΔT_{hyst} , has been identified as the reason for this irreversibility. Moreover, with non-stoichiometric V addition, T_t can be tuned towards room temperature; ΔT_{hyst} , and ΔV can be reduced while maintaining a reasonably large value of ΔS_M and a moderate value of ΔT_{ad} , making this study important for magnetic refrigeration applications and sustainable energy solutions.

ACKNOWLEDGMENTS

The authors thank the Swedish Foundation for Strategic Research (SSF), project “Magnetic materials for green energy technology” (contract EM–16–0039) for financial support. The authors acknowledge support from STandUPP and eSENCE. The computational studies were performed on resources provided by the National Academic Infrastructure for Supercomputing in Sweden (NAISS). S.G., F.S., O.G., and M.S. thankfully acknowledge the financial support of the German Research Foundation (DFG) in the framework of the Collaborative Research Centre Transregio 270 (CRC-TRR 270). O.E. acknowledges support from WISE, Wallenberg Initiative Materials Science. S.G. is thankful to Dr. Konstantin Skokov for helping in measuring the adiabatic temperature change.

- [1] D. Coulomb, J. Dupont, A. Pichard, 29th informatory note on refrigeration technologies. the role of refrigeration in the global economy, International Institute of Refrigeration: Paris, France (2015).
- [2] D. Coulomb, J. Dupont, V. Morlet, The impact of the refrigeration sector on climate change, 35th Note on Refrigeration Technologies (International Institute of Refrigeration, 2017) (2017).
URL <https://inis.iaea.org/Search/51010282>

- [3] K. Gschneidner, V. Pecharsky, Thirty years of near room temperature magnetic cooling: Where we are today and future prospects, International Journal of Refrigeration 31 (6) (2008) 945–961. doi:<https://doi.org/10.1016/j.ijrefrig.2008.01.004>.
URL <https://www.sciencedirect.com/science/article/pii/S0140700708000236>
- [4] O. Gutfleisch, T. Gottschall, M. Fries, D. Benke, I. Radulov, K. P. Skokov, H. Wende, M. Gruner, M. Acet,

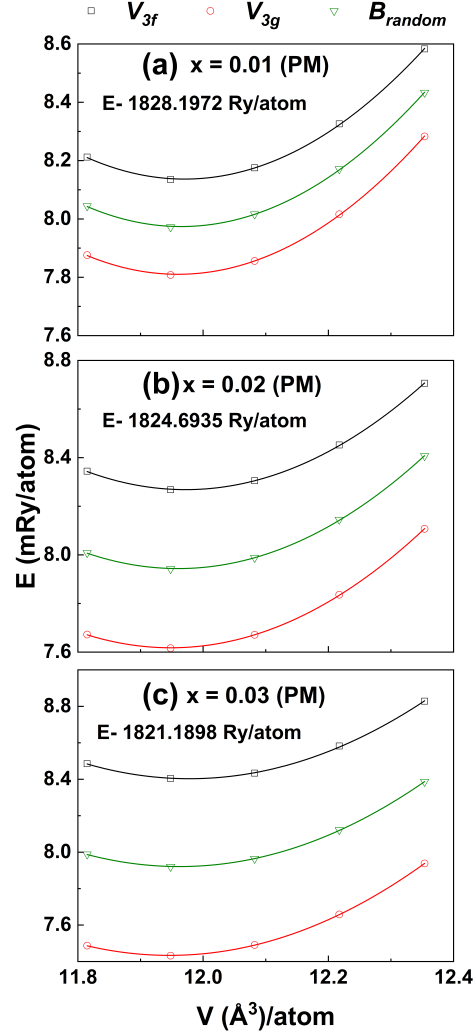
- P. Entel, M. Farle, Mastering hysteresis in magnetocaloric materials, *Philosophical Transactions of the Royal Society A: Mathematical, Physical and Engineering Sciences* 374 (2074) (2016) 20150308. doi:10.1098/rsta.2015.0308.
URL <https://royalsocietypublishing.org/doi/abs/10.1098/rsta.2015.0308>
- [5] F. Zhang, I. Batashev, Q. Shen, Z. Wu, R. I. Smith, G. A. de Wijs, N. van Dijk, E. Brück, Impact of f and s doping on (mn, fe) 2 (p, si) giant magnetocaloric materials, *Acta Materialia* (2022) 118057doi:<https://doi.org/10.1016/j.actamat.2022.118057>.
URL <https://www.sciencedirect.com/science/article/pii/S1359645422004384>
- [6] A. Fujita, Y. Akamatsu, K. Fukamichi, Itinerant electron metamagnetic transition in la (fe x si 1- x) 13 intermetallic compounds, *Journal of Applied Physics* 85 (8) (1999) 4756–4758. doi:10.1063/1.370471.
URL <https://doi.org/10.1063/1.370471>
- [7] T. Krenke, E. Duman, M. Acet, E. F. Wassermann, X. Moya, L. Mañosa, A. Planes, Inverse magnetocaloric effect in ferromagnetic ni–mn–sn alloys, *Nature materials* 4 (6) (2005) 450–454.
URL <https://doi.org/10.1038/nmat1395>
- [8] J. Liu, Y. Gong, Y. You, X. You, B. Huang, X. Miao, G. Xu, F. Xu, E. Brück, Giant reversible magnetocaloric effect in mnnige-based materials: Minimizing thermal hysteresis via crystallographic compatibility modulation, *Acta Materialia* 174 (2019) 450–458. doi:<https://doi.org/10.1016/j.actamat.2019.05.066>.
URL <https://www.sciencedirect.com/science/article/pii/S1359645419303581>
- [9] S. Ghorai, Direct and indirect magnetocaloric properties of first-and second-order phase transition materials, Ph.D. thesis, *Acta Universitatis Upsaliensis* (2022).
URL <https://www.diva-portal.org/smash/record.jsf?dswid=-2441&pid=diva2%3A1706621>
- [10] F. Scheibel, T. Gottschall, A. Taubel, M. Fries, K. P. Skokov, A. Terwey, W. Keune, K. Ollefs, H. Wende, M. Farle, M. Acet, O. Gutfleisch, M. E. Gruner, Hysteresis design of magnetocaloric materials—from basic mechanisms to applications, *Energy Technology* 6 (8) (2018) 1397–1428. doi:<https://doi.org/10.1002/ente.201800264>.
URL <https://onlinelibrary.wiley.com/doi/abs/10.1002/ente.201800264>
- [11] S. Ghorai, J. Cedervall, R. Clulow, S. Huang, T. Ericsson, L. Häggström, V. Shtender, E. K. Delczeg-Czirjak, L. Vitos, O. Eriksson, M. Sahlberg, P. Svedlindh, Site-specific atomic substitution in a giant magnetocaloric fe 2 p-type system, *Physical Review B* 107 (10) (2023) 104409. doi:10.1103/PhysRevB.107.104409.
URL <https://link.AmericanPhysicalSociety.org/doi/10.1103/PhysRevB.107.104409>
- [12] F. Zhang, I. Batashev, N. van Dijk, E. Brück, Effect of off-stoichiometry and ta doping on fe-rich (mn, fe) 2 (p, si) based giant magnetocaloric materials, *Scripta Materialia* 226 (2023) 115253. doi:<https://doi.org/10.1016/j.scriptamat.2022.115253>.
URL <https://www.sciencedirect.com/science/article/pii/S1359646222007473>
- [13] V. Höglin, J. Cedervall, M. S. Andersson, T. Sarkar, M. Hudl, P. Nordblad, Y. Andersson, M. Sahlberg, Phase diagram, structures and magnetism of the femnp 1- x si x-system, *Rsc Advances* 5 (11) (2015) 8278–8284. doi:10.1039/C4RA15419C.
- [14] N. H. Dung, Z. Q. Ou, L. Caron, L. Zhang, D. T. C. Thanh, G. A. De Wijs, R. A. De Groot, K. J. Buschow, E. Brück, Mixed magnetism for refrigeration and energy conversion, *Advanced Energy Materials* 1 (6) (2011) 1215–1219. doi:<https://doi.org/10.1002/aenm.201100252>.
URL <https://onlinelibrary.wiley.com/doi/abs/10.1002/aenm.201100252>
- [15] E. K. Delczeg-Czirjak, L. Bergqvist, O. Eriksson, Z. Gercsi, P. Nordblad, L. Szunyogh, B. Johansson, L. Vitos, Microscopic theory of magnetism in the magnetocaloric material fe₂p_{1-x}t_x (T = B and si), *Physical Review B* 86 (4) (2012) 045126.
URL <https://doi.org/10.1103/PhysRevB.86.045126>
- [16] A. A. Coelho, *TOPAS and TOPAS-Academic*: an optimization program integrating computer algebra and crystallographic objects written in C++, *Journal of Applied Crystallography* 51 (1) (2018) 210–218. doi:10.1107/S1600576718000183.
URL <https://doi.org/10.1107/S1600576718000183>
- [17] J. Liu, T. Gottschall, K. P. Skokov, J. D. Moore, O. Gutfleisch, Giant magnetocaloric effect driven by structural transitions, *Nature materials* 11 (7) (2012) 620–626.
URL <https://www.nature.com/articles/nmat3334>
- [18] P. Hohenberg, W. Kohn, Inhomogeneous electron gas, *Physical review* 136 (3B) (1964) B864. doi:10.1103/PhysRev.136.B864.
URL <https://link.aps.org/doi/10.1103/PhysRev.136.B864>
- [19] L. Vitos, *Computational quantum mechanics for materials engineers: the EMTO method and applications*, Springer Science & Business Media, 2007. doi:<https://doi.org/10.1007/978-1-84628-951-4>.
- [20] J. P. Perdew, Y. Wang, Accurate and simple analytic representation of the electron-gas correlation energy, *Physical review B* 45 (23) (1992) 13244. doi:10.1103/PhysRevB.45.13244.
URL <https://link.aps.org/doi/10.1103/PhysRevB.45.13244>
- [21] J. P. Perdew, K. Burke, M. Ernzerhof, Generalized gradient approximation made simple, *Physical review letters* 77 (18) (1996) 3865. doi:10.1103/PhysRevLett.77.3865.
URL <https://link.aps.org/doi/10.1103/PhysRevLett.77.3865>
- [22] P. Soven, Coherent-potential model of substitutional disordered alloys, *Physical Review* 156 (3) (1967) 809. doi:10.1103/PhysRev.156.809.
URL <https://link.aps.org/doi/10.1103/PhysRev.156.809>
- [23] B. Gyorffy, A. Pindor, J. Staunton, G. Stocks, H. Winter, A first-principles theory of ferromagnetic phase transitions in metals, *Journal of Physics F: Metal Physics* 15 (6) (1985) 1337. doi:10.1088/0305-4608/15/6/018.
URL <https://dx.doi.org/10.1088/0305-4608/15/6/018>
- [24] V. Höglin, M. Hudl, M. Sahlberg, P. Nordblad, P. Beran, Y. Andersson, The crystal and magnetic structure of the magnetocaloric compound femnp_{0.5}si_{0.5}, *Journal of Solid State Chemistry* 184 (9) (2011) 2434–2438. doi:<https://doi.org/10.1016/j.jssc.2011.06.019>.
URL <https://www.sciencedirect.com/science/>

- article/pii/S0022459611003458
- [25] L. Pal, K. Suresh, A. Nigam, Effect of mn substitution on the magnetic and magneto-transport properties of fe₃-xmnxsi (0 < x < 1.25) alloys, *Journal of Applied Physics* 113 (9) (2013).
URL <https://doi.org/10.1063/1.4794126>
- [26] D. Cam Thanh, E. Brück, N. Trung, J. Klaasse, K. Buschow, Z. Ou, O. Tegus, L. Caron, Structure, magnetism, and magnetocaloric properties of mn fe p 1- x si x compounds, *Journal of Applied Physics* 103 (7) (2008) 07B318. doi:10.1063/1.2836958.
URL <https://doi.org/10.1063/1.2836958>
- [27] B. Carlsson, M. Gölin, S. Rundqvist, Determination of the homogeneity range and refinement of the crystal structure of fe₂p, *Journal of Solid State Chemistry* 8 (1) (1973) 57–67. doi:[https://doi.org/10.1016/0022-4596\(73\)90021-2](https://doi.org/10.1016/0022-4596(73)90021-2).
URL <https://www.sciencedirect.com/science/article/pii/0022459673900212>
- [28] K. A. Gschneidner, V. Pecharsky, A. Tsokol, Recent developments in magnetocaloric materials, *Reports on progress in physics* 68 (6) (2005) 1479. doi:10.1088/0034-4885/68/6/R04.
URL <https://dx.doi.org/10.1088/0034-4885/68/6/R04>
- [29] S. Ghorai, D. Hedlund, M. Kapuscinski, P. Svedlindh, A setup for direct measurement of the adiabatic temperature change in magnetocaloric materials, *IEEE Transactions on Instrumentation and Measurement* 72 (2023) 1–9. doi:10.1109/TIM.2023.3272387.
- [30] A. M. Tishin, Y. I. Spichkin, *The magnetocaloric effect and its applications*, CRC Press, 2016. doi:<https://doi.org/10.1201/9781420033373>.
- [31] M. Fries, L. Pfeuffer, E. Bruder, T. Gottschall, S. Ener, L. V. Diop, T. Gröb, K. P. Skokov, O. Gutfleisch, Microstructural and magnetic properties of mn-fe-p-si (fe₂ p-type) magnetocaloric compounds, *Acta Materialia* 132 (2017) 222–229. doi:<https://doi.org/10.1016/j.actamat.2017.04.040>.
URL <https://www.sciencedirect.com/science/article/pii/S1359645417303348>
- [32] Z. Zheng, H. Wang, C. Li, X. Chen, D. Zeng, S. Yuan, Enhancement of magnetic properties and magnetocaloric effects for mn_{0.975}fe_{0.975}p_{0.5}si_{0.5} alloys by optimizing quenching temperature, *Advanced Engineering Materials* 25 (5) (2023) 2200160.
URL <https://doi.org/10.1002/adem.202200160>
- [33] N. V. Thang, N. H. v. Dijk, E. Brück, Tuneable giant magnetocaloric effect in (mn, fe) ₂ (p, si) materials by co-b and ni-b co-doping, *Materials* 10 (1) (2016) 14.
URL <https://www.mdpi.com/1996-1944/10/1/14>
- [34] H. Yibole, F. Guillou, L. Zhang, N. Van Dijk, E. Brück, Direct measurement of the magnetocaloric effect in mnfe (p, x)(x= as, ge, si) materials, *Journal of Physics D: Applied Physics* 47 (7) (2014) 075002.
URL <https://dx.doi.org/10.1088/0022-3727/47/7/075002>
- [35] S. Ghorai, R. Skini, D. Hedlund, P. Ström, P. Svedlindh, Field induced crossover in critical behaviour and direct measurement of the magnetocaloric properties of la_{0.4}pr_{0.3}ca_{0.1}sr_{0.2}mno₃, *Scientific Reports* 10 (1) (2020) 1–13.
URL <https://doi.org/10.1038/s41598-020-76321-w>
- [36] K. Gschneidner Jr, V. K. Pecharsky, Magnetocaloric materials, *Annual Review of Materials Research* 30 (2000) 387.
URL <https://doi.org/10.1146/annurev.matsci.30.1.387>
- [37] J. Liu, M. Krautz, K. Skokov, T. G. Woodcock, O. Gutfleisch, Systematic study of the microstructure, entropy change and adiabatic temperature change in optimized la–fe–si alloys, *Acta Materialia* 59 (9) (2011) 3602–3611. doi:<https://doi.org/10.1016/j.actamat.2011.02.033>.
URL <https://www.sciencedirect.com/science/article/pii/S1359645411001273>
- [38] T. Gottschall, K. P. Skokov, B. Frincu, O. Gutfleisch, Large reversible magnetocaloric effect in Ni-Mn-In-Co, *Applied Physics Letters* 106 (2) (2015) 021901. doi:10.1063/1.4905371.
URL <https://doi.org/10.1063/1.4905371>
- [39] M. Hudl, L. Häggström, E.-K. Delczeg-Czirjak, V. Höglin, M. Sahlberg, L. Vitos, O. Eriksson, P. Nordblad, Y. Andersson, Strongly enhanced magnetic moments in ferromagnetic femnp_{0.5}si_{0.5}, *Applied Physics Letters* 99 (15) (2011). doi:10.1063/1.3651272.
URL <https://doi.org/10.1063/1.3651272>

SUPPLEMENTARY INFORMATION (SI)

A. Total energy in the PM state

As described in the main text, the total energy calculation in the FM state indicates a $3g$ site preference of V. The total energy values for the PM state are shown in Fig. 1 (a)-(c). For the details of the V_{3f} , V_{3g} , and B_{ran} cases, see main text.



SI Fig. 1. (a)-(c) The calculated total energy as a function of the lattice volume in the PM state of the studied alloys. The energy values are rescaled (see inset formula) with respect to the minimum total energy of the corresponding alloy. The color coded lines joining the data points are polynomial fits to the corresponding data.

B. Formation energy calculation

To check the phase stability, the phase formation energy calculations have been performed. In order to maintain the Fe₂P-type structure after the addition of FeV in the (Fe, Mn)₂(P, Si) alloy, a vacancy will be created in the P/Si (1b/2c) site. However, there is no such previous experimental evidence for the presence of atomic vacancy in the Fe₂P-type structure. If x amount of FeV is added to $(1-x)$ amount of (Fe, Mn)₂(P, Si) alloy, the V can occupy either the 3g or 3f site in the Fe₂P structure (cf. Fig. 1 (a)). The formation energy for the V occupying the 3g site, has been calculated as,

$$\Delta F_{3g} = \Delta F_{Fe(V_x Mn_{1-x})P_{0.5-x/2}Si_{0.5-x/2}Vac_x} = E_{Fe(V_x Mn_{1-x})P_{0.5-x/2}Si_{0.5-x/2}Vac_x} - E_{Fe} - xE_V - (1-x)E_{Mn} - (0.5-x/2)E_P - (0.5-x/2)E_{Si} - xE_{Vac}.$$

where V_{ac} represents the vacancy. Similarly, the formation energy, corresponding to 3f site occupancy of V, can be calculated as,

$$\Delta F_{3f} = \Delta F_{(Fe_{1-x}V_x)(Fe_x Mn_{1-x})P_{0.5-x/2}Si_{0.5-x/2}Vac_x} = E_{(Fe_{1-x}V_x)(Fe_x Mn_{1-x})P_{0.5-x/2}Si_{0.5-x/2}Vac_x} - E_{Fe} - xE_V - (1-x)E_{Mn} - (0.5-x/2)E_P - (0.5-x/2)E_{Si} - xE_{Vac},$$

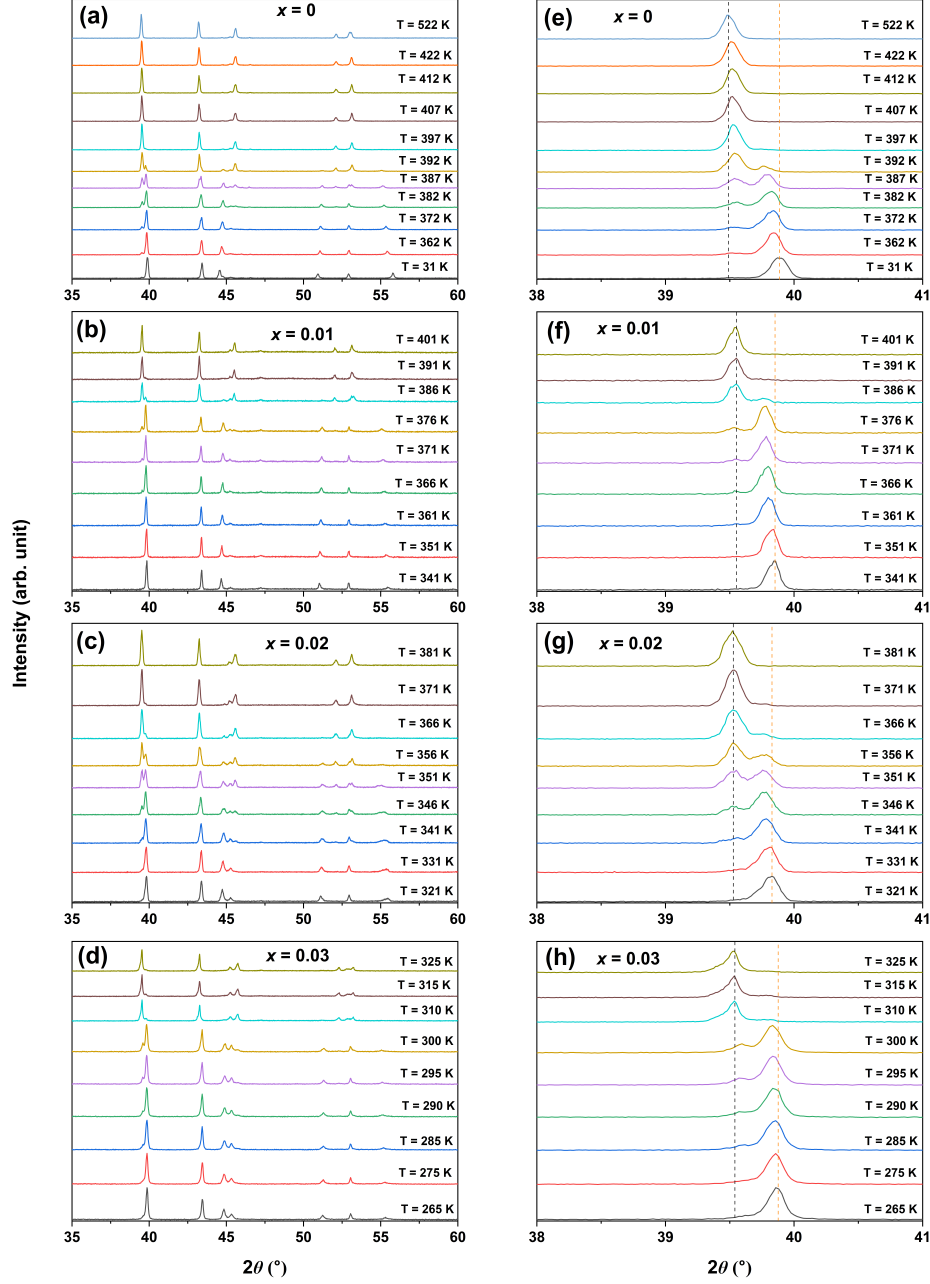
The difference in formation energy (ΔF_{3g-3f}) for V occupying the 3g and 3f sites is shown in SI Table 1 for the ferromagnetic and paramagnetic states. A negative value of ΔF_{3g-3f} indicates a more stable alloy when V occupies the 3g-site. Noticeably, the energy difference ΔF_{3g-3f} increases with the increasing amount of V, i.e. V will be increasingly more stable in the 3g-site with an increasing amount of V.

SI Table 1. Results from formation energy calculations. The energy differences are given in units of mRy/atom.

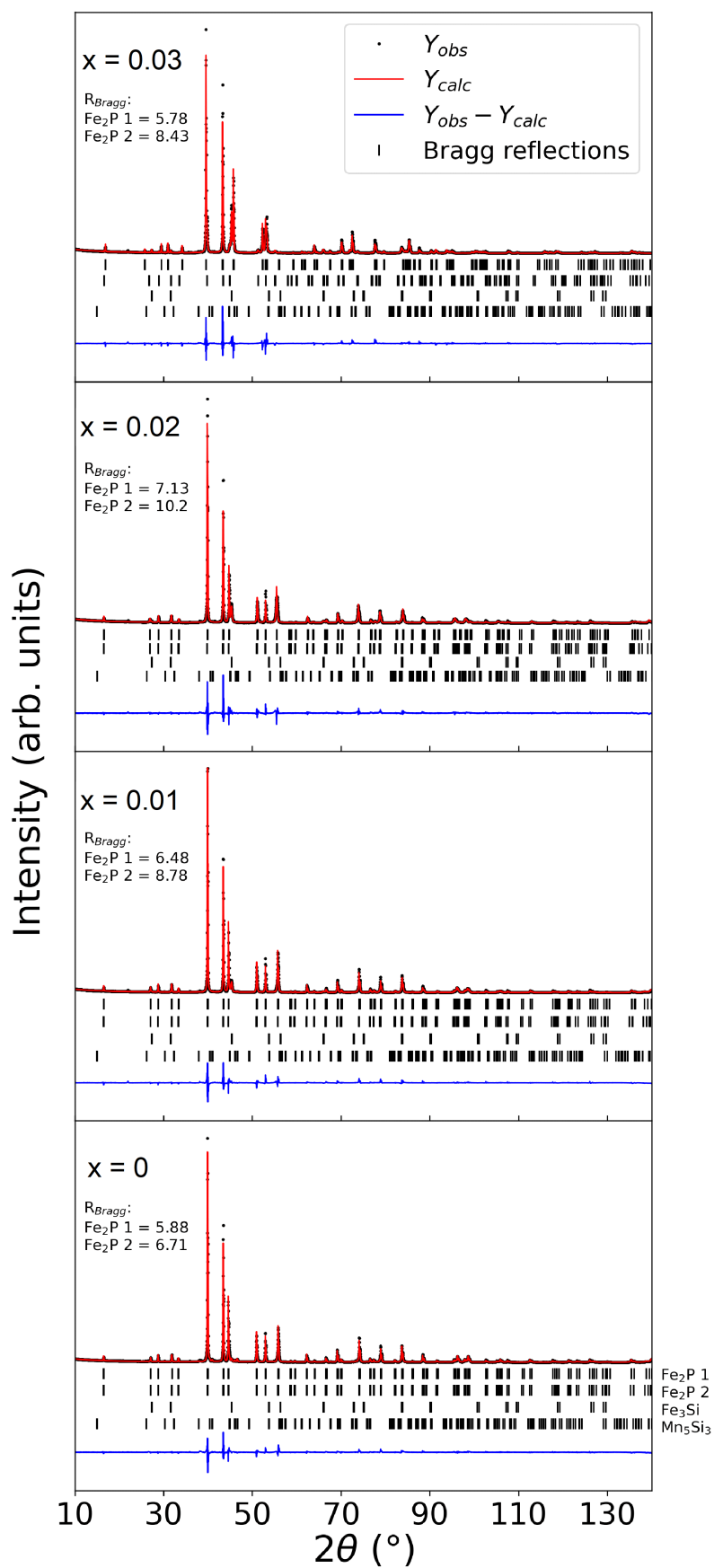
x	FM	PM	FM	PM
	($c/a = 0.53$)	($c/a = 0.53$)	($c/a = 0.5848$)	($c/a = 0.5848$)
0	0	0	0	0
0.01	-0.316	-0.326	-0.370	-0.456
0.02	-0.630	-0.646	-0.751	-0.908
0.03	-0.934	-0.944	-1.103	-1.350

C. Temperature dependent XRPD

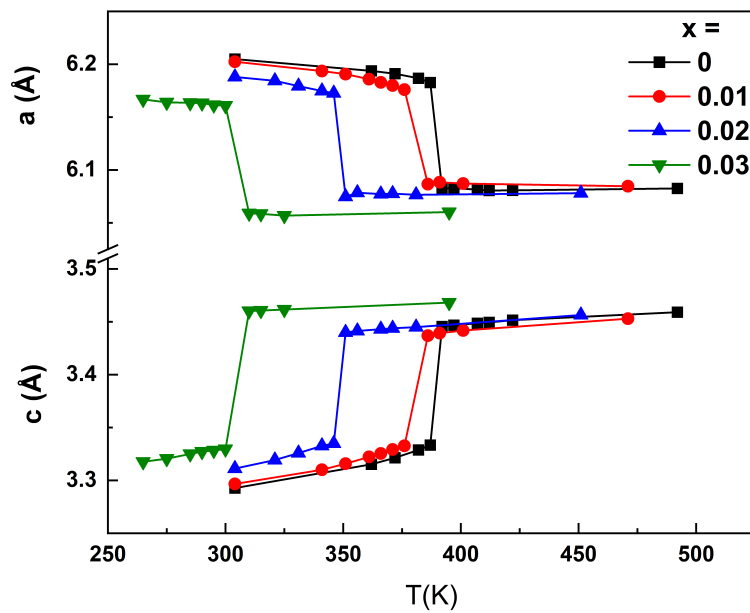
The temperature dependent XRPD patterns for all studied alloys are shown in SI Fig. 2, recorded during heating. In SI Figure2 (e)-(h), the (111) peaks for the hexagonal phases are highlighted with dotted lines. With increasing temperature, this peak shifts towards lower 2θ values indicating a lattice expansion, i.e. a phase change from lower c/a to higher c/a . The Rietveld refinements of the room temperature XRPD patterns are shown in SI Fig. 3. The temperature dependence of the lattice parameters (c , a) of the dominating Fe_2P -phase for the four studied alloys are shown in SI Fig. 4.



SI Fig. 2. Temperature dependent XRPD patterns for the $x =$ (a) 0, (b) 0.01, (c) 0.02, and (d) 0.03 alloys respectively, recorded during heating. (e)-(h) Enlarged XRPD patterns, the dotted lines indicate the peak position for two Fe_2P -type phases with different c/a ratios.



SI Fig. 3. Rietveld refinement of the XRPD patterns of the four studied alloys. Fe_2P1 , and Fe_2P2 are the hexagonal phases with low and high c/a ratios, respectively. The Bragg peaks for the secondary Fe_3Si , and Mn_5Si_3 phases are also shown.



SI Fig. 4. Temperature dependence of the lattice parameters (c , a) of the dominating Fe_2P -phase (wt% > 60%) during heating. The error in the lattice parameter data is in the order of 10^{-4} Å.